UNIVERSITY OF COPENHAGEN
FACULTY OF SCIENCE

MSc in Environmental Science - Soil, Water and Biodiversity (EnvEuro)

Tests investigating potential implementation of oxygen isotope measurements in continuous flow analyses

Bettina Loy

Supervised by Ida Lager and Thomas Blunier

May 2023

Bettina Loy

Tests investigating potential implementation of oxygen isotope measurements in continuous flow analyses

MSc in Environmental Science - Soil, Water and Biodiversity (EnvEuro), May 2023

Supervisors: Ida Lager and Thomas Blunier

University of Copenhagen

Faculty of Science

Masters Degree in Environmental Sciences

Blegdamsvej 3B

2200 Copenhagen N

Acknowledgments

A special thanks to Davide, for not only working together with me, but also becoming a great friend! Thanks also to all the other master students and people at PICE, for creating such a nice and fun atmosphere.
Lastly, I want to thank my supervisor Thomas Blunier, Michael Döring and Michael Dyonisius for the great support throughout this thesis.
And most importantly, thank you Thomas for letting us organize the πs day and set-up the foosball table!

Abstract

In addition to the current CFA setup at PICE, a line to measure oxygen isotopes was built. The gas separated from the ice cores flows through a membrane, where oxygen diffuses out and the O_2 depleted sample gets measured in the mass spectrometer. This project aimed to create a second line for the extracted oxygen to be measured. Experiments were taken to investigate on the reaction time of the line and the permeation process of the membrane. Therefore, firn air bottles with different isotopic compositions were used to compare with the air in the lab. Permeation seems to be dependant on the volume of the wall and inner part of the membrane as well as the surrounding glass tube. While better measurements could be achieved with a thinner and shorter membrane, the results suggest that the membrane fractionates the oxygen to the point, where no difference in samples with varying delta values can be observed.

Abbreviations

BPR	Back pressure regulator
CFA	Continuous flow analysis
FPR	Forward pressure regulator
IRMS	Isotope ratio mass spectrometry
MFC	Mass flow controller
MS	Mass spectrometer
NEEM	North Greenland Eemian deep ice core
PICE	Department for Physics of Ice, Climate and Earth
PID	Proportional – Integral – Derivative

Contents

1 Introduction

The study of paleo-climatic records is crucial to provide insights and understanding of past climate systems, which further helps to ameliorate the prediction of future climate events alike the ongoing global climate crisis (Bradley, 2000). Such records can be lake or oceanic sediments, volcanic debris and the stable isotopic composition of ice or air bubbles trapped within.

1.0.1 Stable isotope studies

Isotopes are atoms with the same number of protons in the nucleus, but a different number of neutrons and therefore they vary in mass. Several natural processes have been found to change the isotopic composition of elements, as heavier isotopes react and behave slightly different than lighter ones. Those processes are called fractionation processes and often represent important physical, chemical or biological activities. Therefore, stable isotope studies are a powerful tool in the research field of Paleoclimatology. The values of isotopic compositions are usually discussed in delta δ, which is based on the ratios R of less compared to more abundant isotopes such as

$$R = \frac{^{18}O}{^{16}O}$$

for oxygen stable isotopes. As those ratios are very small numbers and the absolute values are difficult to measure, the delta notation is calculated by comparing R to a standard value R_S and its deviation from unity

$$\delta = \left[\frac{R}{R_s} - 1\right].$$

The isotope ratios are commonly specified by indicating the rare isotope, i.e. $\delta^{18}O$ for $^{18}O/^{16}O$. Furthermore, delta notation is also often used to describe ratios between different elements or molecules such as O_2/N_2 (Cuffey & Paterson, 2010).

1.0.2 Firn and ice

Firn is a intermediate form between snow and glacial ice and is formed via densification by the weight of new layers of snow accumulating above (Herron & Langway, 1980). This process results in a porous firn-layer of 50 - 100 m thickness (Severinghaus et al., 2001), which can be divided into three zones based on the predominant gas transport: the convective zone, the diffusive zone and the non-diffusive/ lock-in zone, the latter being the deepest.

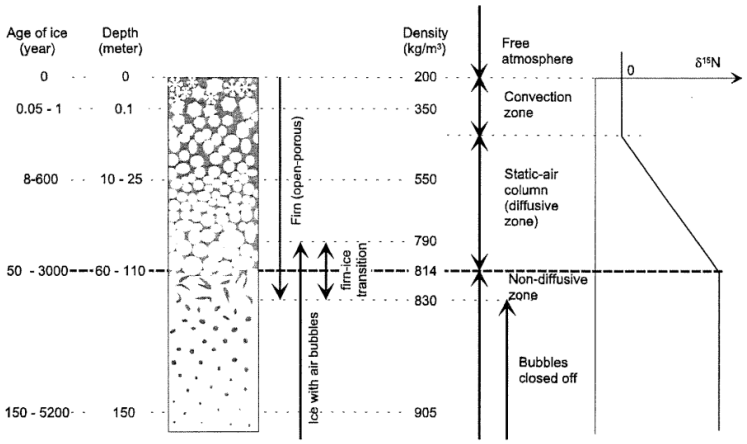

Figure 1.1: Sketch of the firn column. The indicated depths and age ranges are typical for polar ice sheets. Air bubbles mainly form at densities between 790 and 830 kg/m^3. Depth and correlating densities of the firn and ice are depicted to the left. Subdivision into zones suggested by Sowers et al. (1992) are given on the right side. From Blunier and Schwander (2000).

The layers closest to the surface still resemble snow in regards to density and structure, while the air within can exchange freely with the surface, controlled by wind. Further down the permeability of the gases through the firn decreases and processes such as gravitational and thermal fractionation control the isotopic composition. The lock-in zone is as the name suggest the layer in which the gas finally gets trapped as bubbles form in the ice structure when density reaches about 814 $\frac{kg}{m^{-3}}$ (see figure 1.1). The transition from firn to ice is considered around the non-diffusive zone. Overall, the bubbles preserve the atmospheric compositions of gases such as CO_2 and CH_4 due to

the fact that the natural sinks of those gases don't affect them once they are trapped in the ice (Buizert et al., 2012; Cuffey & Paterson, 2010).

1.0.3 Ice core studies

Not only firn (air) can be studied, but also deeper levels can be reached by drilling several thousand meters into glaciers in projects like the North Greenland Eemian Ice Drilling NEEM (Dahl-Jensen et al., 2002) or the North Greenland Icecore Project NorthGRIP/NGRIP (Rasmussen et al., 2013). The yearly accumulation of snow and ice on a glacier provides a pure record on environmental conditions of the past, so long periods can be studied. While the gas content in bubbles directly reflects past conditions, isotopic compositions are indirectly influenced by environmental variables (Cuffey & Paterson, 2010) and act as proxies. This means, that they are linked to other factors such as temperature and can be used as indicators for variables which cannot be measured directly.

1.0.4 Fractionation

The composition of oxygen isotopes in firn air does not directly represent the past atmosphere, as the molecules are affected by different processes until being locked off in the ice. Fractionation occurs in the diffusive zone of the firn layer and due to the fact that lighter molecules require less energy to move around compared to the heavier ones. There are two types of fractionation occurring in firn: gravitational and thermal fractionation.

1. Gravitational fractionation
Heavier isotopes are affected more by gravitation than lighter ones and thus, they accumulate at the bottom of the firn air column. Molecular diffusion driven by a concentration gradient acts as a counter-force to gravitation and an equilibrium is reached when both are in balance (Craig et al., 1988; Schwander et al., 1993).

2. Thermal fractionation
Temperature differences within the firn layer cause additional fractionation. As it is colder at the bottom and heavier molecules tend to migrate away from heat, this process causes additional accumulation of heavy isotopes with depth. Especially for a rapid increase in temperature this effect is stronger, creating a record for abrupt climate changes (Severinghaus et al., 2001). As with gravitational diffusion, an equilibrium is reached when the effect is in balance with molecular diffusion (Grew and Ibbs, 1952, in Severinghaus et al., 1998, p.2).

1.0.5 Oxygen isotopes

Oxygen is the second most abundant gas in the atmosphere (20.8%) and especially interesting in climatology, as it plays a key role in many parts of the Earth's climate system. The three stable isotopes of oxygen are ^{16}O (99.762%), ^{17}O (0.038%) and $_{18}$O (0.200%). As aforementioned, the lighter isotopes interact slightly different compared to heavier ones, so their composition is influenced by various factors. One effect caused by fractionation is known as the Dole effect, which describes the difference in $\delta^{18}O$ between seawater and atmospheric O_2(Dole, 1935). This phenomenon is first and foremost caused by respiration of plants and animals, which take up preferably the lighter isotope $\delta^{16}O$ and thus decrease its relative abundance in the air. Factors like precipitation and temperature affect primary production on land and in the sea, leading to $\delta^{18}O$ values being linked to the global climate. Several studies have indicated a causality of past abrupt climate changes on the Dole effect (Bender et al., 1994; Malaizé et al., 1999; Severinghaus et al., 2009).

Water is the one source for all oxygen on Earth and henceforth, the oxygen and water cycles are linked through various biogeochemical processes. One

important fractionation process within the water cycle is known as Rayleigh distillation:

As shown in figure 1.2, seawater evaporates and the vapour is depleted form heavy isotopes, as they prefer the liquid phase. The $\delta^{18}O$ values of the cloud are hence smaller compared to the ocean. When those clouds then move towards land or higher latitudes and precipitation occurs, the rain will be enriched in heavy isotopes, while the vapour continuously get lighter. The further away from the source, the stronger this effect. If the temperature increases, more water evaporates from the sea and the vapour has higher $\delta^{18}O$ values than during a colder climate. When precipitation sets in again, the rain will now be enriched in more heavy isotopes compared to the situation with lower temperatures. Consequently, factors such as the distance from the source, precipitation and global temperatures affect the isotopic footprint of water on land. Additionally, once the water reaches land, evapotranspiration causes further fractionation. Evaporation from soil, water bodies and canopy as well as transpiration from plants releases lighter water vapor into the air. Its $\delta^{18}O$ value consequently decreases with rising evapotranspiration which is in turn positively related to heat and low humidity.
Plant roots now take up the water with the isotopic composition characterized by those effects and use it during photosynthesis to produce glucose and oxygen, a process which has been proven to not cause additional fractionation. The $\delta^{18}O$ value in the atmosphere is consequently impacted by the isotopic composition of the water taken up by plants. However, this effect is much smaller than the impact of respiration and accounts for only a small share of oxygen fractionation (Blunier & Leuenberger, 2008).
In conclusion, oxygen deltas in the atmosphere are linked to the global climate due to the amount of primary production and corresponding respiration and furthermore, Rayleigh distillation and evapotranspiration influencing the isotopic composition of oxygen in water, which is being taken up by plants and then released into the atmosphere during photosynthesis. When measuring isotopic compositions in ice cores, conclusions about past conditions such as global primary production can only be drawn once the fractionation processes (chapter 1.0.4) within the ice and firn are accounted for (Blunier & Leuenberger, 2008; Dansgaard, 2012; Pederzani & Britton, 2019).

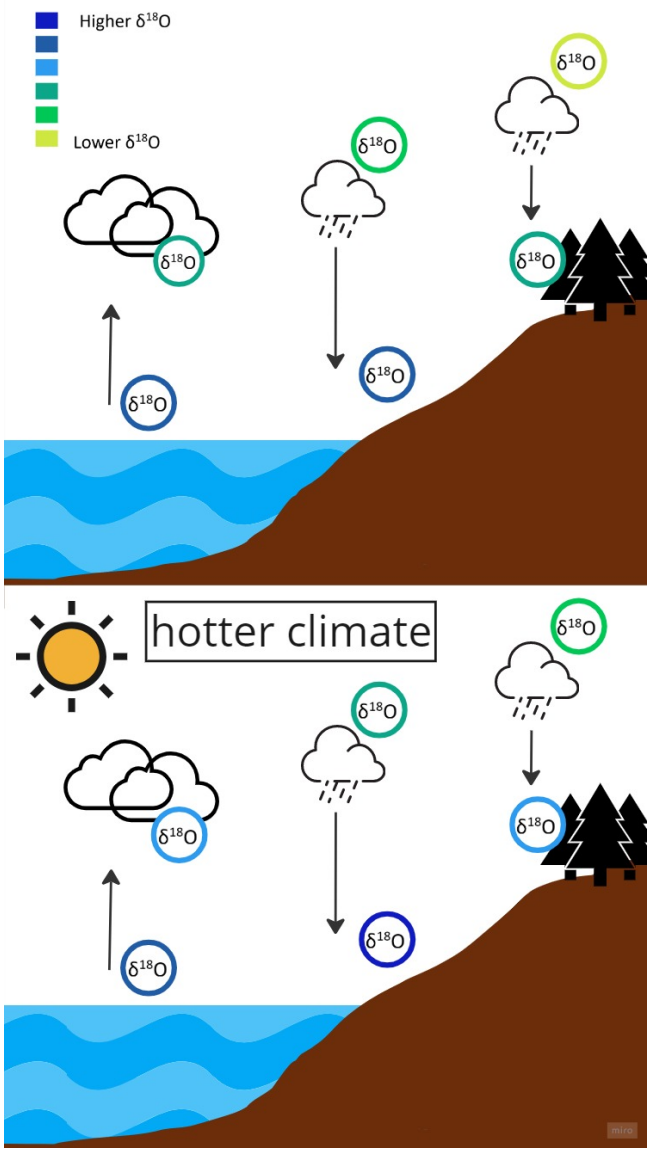

Figure 1.2: Rayleigh fractionation: water vapour gets depleted from heavy oxygen isotopes further from the source. Precipitation is enriched in heavy isotopes and increased temperatures lead to overall higher $\delta^{18}O$ values in water on land.

Materials and Methods

2

2.1 Materials

2.1.1 Mass spectrometer

The mass spectrometer (MS) measures the mass-to-charge ratio of ions. Firstly, the gas to be measured enters through a gas inlet system at a pressure in the range of 10^{-6} to 10^{-8} mbar. The sample then enters the ionization chamber as seen in 2.1, where a heated filament is releasing electrons perpendicular to the to the gas flow. The molecules hit by those electrons consequently get stripped of an electron from their electron cloud and ionize positively (ionization). The now cations are further channeled through electric plates and accelerated before entering a magnetic field to get deflected (acceleration). The molecule are mostly simple ionised, causing their mass-to-charge ratio to be dependant on their mass, which in turn defines their path of deflection. Heavier cations are deflected in a different radius than lighter ones with the same charge (deflection). Finally, the ion beams hit different so-called Faraday cups, positioned to catch cations of specific masses. The amount of ions can now be detected, as moving ions correspond to an electric current, which is firstly amplified and then measured in Volt over an electric resistance (detection). Depending on the abundance of the ions, different resistors are used to ensure a resulting voltage within a similar range (Blunier & Leuenberger, 2008).

The masses the MS is set to measure are shown in table 2.1. Each mass corresponds to various molecules and the most common and relevant for this thesis are listed.

Figure 2.1: The principle of a mass spectrometer. It can be switched between sample and reference to enter the gas inlet through a capillary. From Guillevic (2013).

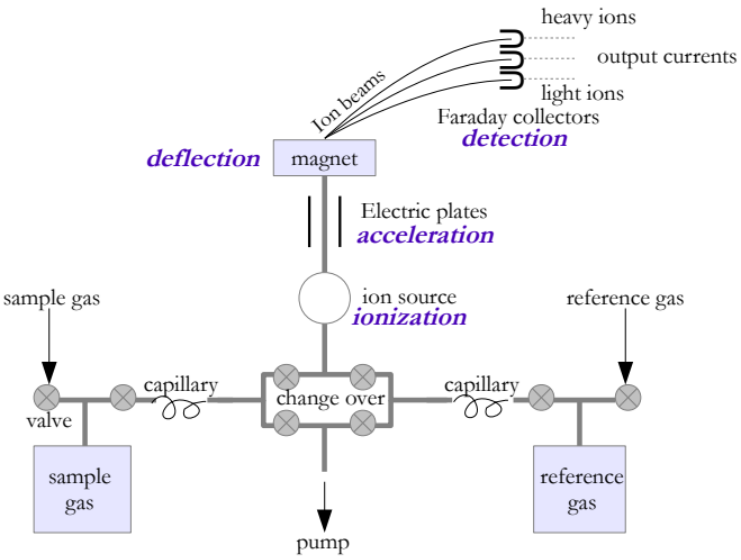

Table 2.1: Masses that can be measured in the MS. Different configurations have to be chosen depending on the desired molecule, as not all masses can be measured at once. Rare isotopes are indicated by their mass, which is super scripted.

Mass	Molecule	
28	Nitrogen	N_2
29	Nitrogen	$^{29}N_2$
30	Nitrogen, Nitric Oxide, ...	$^{30}N_2$, NO
31	Phosphorus, ...	P
32	Oxygen	O_2
33	Oxygen	$^{33}O_2$
34	Oxygen	$^{34}O_2$
36	Argon and Oxygen	^{36}Ar, $^{36}O_2$
40	Argon	Ar
44	Carbon dioxide	CO_2

The measurements of molecules with the same masses interfere; it is therefore useful to separate the sample. When reading the mass spectrometry measurements, one can choose between different configurations, because the MS cannot measure all masses simultaneously. The configurations used for this thesis were AIR and O2, measuring the following masses:

AIR	28, 29, 30, 32, 36, 40, 44
O2	32, 33, 34

It is additionally important to mention, that all masses have a specific resistor, which ensures that the results can be visualized in one graph, as the maximum signal to be shown is 50 V. Every configuration (such as AIR and O2 as used in this project) has a specific resistor configuration and to compare the concentrations of different gases its is crucial to take those resistors into account, which can be found in table 2.2 and 2.3. If there is another configuration for which the mass has a higher resistor, it is possible to set it to 'high amplification' when the values are very low.

Table 2.2: Cup configuration settings for the O2 configuration. An 'X' in the high amp. row indicates that there is no higher resistor and high amplification is not possible.

Mass	**32**	**33**	**34**
Resistor	3×10^{8}	3×10^{11}	1×10^{11}
High amp.	1×10^{11}	X	X

Table 2.3: Cup configuration settings for the AIR configuration.

Mass	**28**	**29**	**30**	**32**	**36**	**40**	**44**
Resistor	3×10^{8}	3×10^{10}	1×10^{11}	1×10^{9}	1×10^{12}	1×10^{10}	3×10^{11}
High amp.	1×10^{9}	1×10^{11}	X	1×10^{11}	X	X	X

2.1.2 Perovskite membrane

The name refers to various compounds with a crystal structure corresponding to the one of calcium titanium oxide mineral. Perovskite membranes are 100% selective to O_2 permeability and are therefore commonly used for applications such as air separation and oxygen production (Liang et al., 2010). For this thesis, tubular perovskite membranes of the chemical composition $BaCO_xFe_yZr_{1-x-y}O_{3-\delta}$ (BCFZ) were used to extract oxygen from the samples. They are provided by *Fraunhofer-Institute for Interfacial Engineering and Biotechnology Inorganic Surfaces and Membranes* and developed using a phase inversion spinning process followed by sintering. The inner diameter of the membrane was about 0.8 mm and the outer diameter around 1.1 mm. The permeation process consists of

1. the exchange of molecular oxygen and oxygen ions on the inner membrane surface
2. bulk diffusion of the oxygen ion
3. the surface-exchange reaction on the outer side

(Jiang et al., 2010; Yang et al., 2005). The oxygen diffusion is driven by a partial pressure difference between inside and outside of the membrane as shown in figure 2.2 and highly linked to temperature, previously used at 850 °C (Liisberg, 2020) for the same setup as this project.

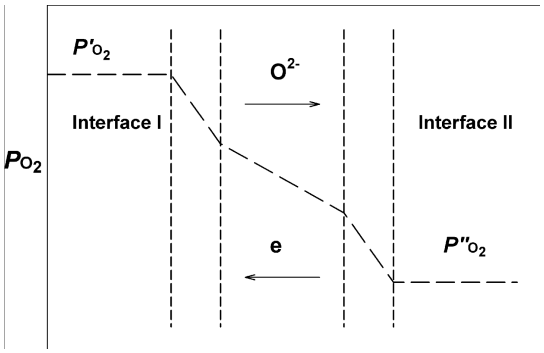

Figure 2.2: Partial pressure differences for the sections involved in the oxygen permeation process. Permeation is caused by a partial pressure gradient between interface I and II as well as the surface exchange reaction. From Sunarso et al. (2008).

2.2 Experimental setup

2.2.1 Continuous flow analysis system

The goal of the work presented here is to perform a continuous flow analysis (CFA) on ice cores and furthermore attempt to measure O_2 isotopic ratios, which was not possible with the initial setup. The latter consists of a freezer in which the ice-core to be analysed is slowly melted on a heated unit called melt-head and a following gas line to extract the gases of interest (figure 2.3). Multiple pressure and flow regulators are included in the setup to create pressure gradients and a direction of flow towards the mass spectrometer. There are three types of regulators:

1. mass flow controller regulating the flow in ml/min directly
2. forward pressure regulator controlling the pressure of the outgoing flow
3. back pressure regulator controlling the pressure of the in-going flow

Only the central part of the ice cores is used for further analysis, while the outside directly flows into waste. The line from the center of the melt-head continues to the Debubbler, where the bubbles are separated from the water, which then is part of the dust line, which is not analysed in this project. From there on, the line passes two three-port valves. The second one can be switched to measure Glacial and Holocene standards, which flow into waste at the set-up shown in 2.3. After the second valve with the bypass, the line enters a Membrane to separate gas from water and continues as a gas-line in a steel tube. The three triangles also represent a valve, where black filling indicates a flow and white means it is closed at that side. As the goal of this project is mainly to improve the CFA rather than measure real samples, the line is neither connected with the freezer nor with the N_2/Ar mixture on the sample side, but usually open to measure lab air or bottles with air samples from Greenland. Following the upper valve is the first T separating the line towards the Picarro and the MS. A pressure regulator is connected to the T and set to 300 mbar. Both lines continue into a Nafion tube, a short and a long one; but with the same purpose: to further dry the sample and ensure all water vapor is removed. The Nafion tubes are both connected to helium, which is used as a sweep-gas. From the long Nafion, the line continues to the Flow-meter, and then enters the Picarro, where the methane concentration

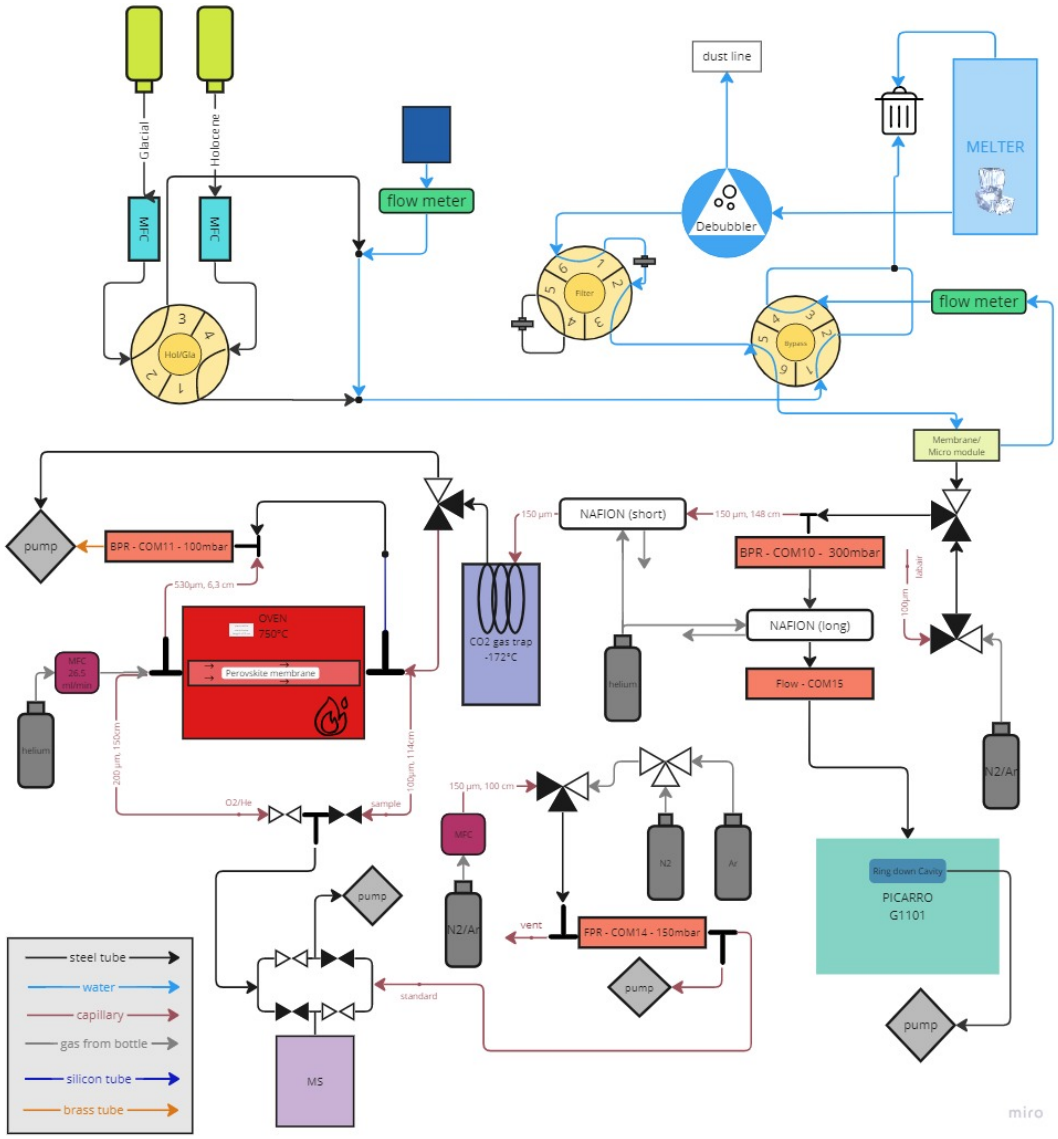

Figure 2.3: Final setup of the CFA. BPR: back pressure regulator, MFC: mass flow controller, FPR: forward pressure regulator. The COM numbers are the corresponding connections to the computer visible on LabView. Different colors correspond to various kinds of tubes as depicted in the legend. The set up was slightly changed for some experiments. The water line before the Micro module was not used for this thesis. The carbon dioxide was freezed out in the trap several times, but not continuously.

is measured. All automatic valves, mass flow controllers and meters, back- and front-pressure regulators are controlled or monitored by the program LabView with a graphical user interface. This program provided a data sheet containing all the monitored data with a 1s frequency. The part that entered the long Nation flows instead into the CO_2-trap, where this gas can be frozen out via liquid nitrogen (this was only used a few times during this project). The following valve is either set for the sample to flow further towards the oven or for the CO_2 to leave the trap towards a pump. After using the trap, it has to be emptied from the accumulated CO_2, before the valve can be set towards the oven again. The process within the oven is the major part of the thesis and described later on in 2.2.2. In a nutshell, O_2 is removed with helium again as a sweep-gas (entering left of the oven) and the line leaves in a different capillary, next to where it entered, but depleted from oxygen. From there, the line enters the MS.

The purpose of the oven before the MS is to extract O_2, as the heavy isotope $^{18}O_2$ otherwise interferes with the data for ^{36}Ar, which has the same mass. The set-up of the oven is as follows: the sample flows into a Perovskite-membrane which is uniquely permeable for O_2 at temperatures above approximately 550 °C. The oxygen is then flushed away with helium and pumped out.

2.2.2 Oxygen removal

The goal of this project was to find a way to create a line for the helium and O_2 mix going into the MS, so that via a valve, one could switch between measuring oxygen isotopes and the initial gas mixture. As shown in figure 2.4, the sample line enters the perovskite membrane in the oven, which is controlled by a PID temperature controller. The latter is connected to a thermocouple, which is placed in the center of the oven and the temperature is set to 750 °C. The oxygen then passes through the membrane, and gets flushed away with helium. As the membrane is selective to oxygen, the gas mixture outside of the membrane consists only of oxygen and helium, free of any other component. At the left end the membrane is sealed with Torr-seal where the oxygen depleted air then enters a capillary and leaves the oven to the MS. The maximum temperature of Torr-seal is 120 °C, so it cannot withstand the heat inside the oven. Hence the length of the membrane is set so it sticks out at both ends, where it can be sealed vacuum-tight. Another capillary was added

from outside in the glass tube where the helium and oxygen flows in towards the MS.

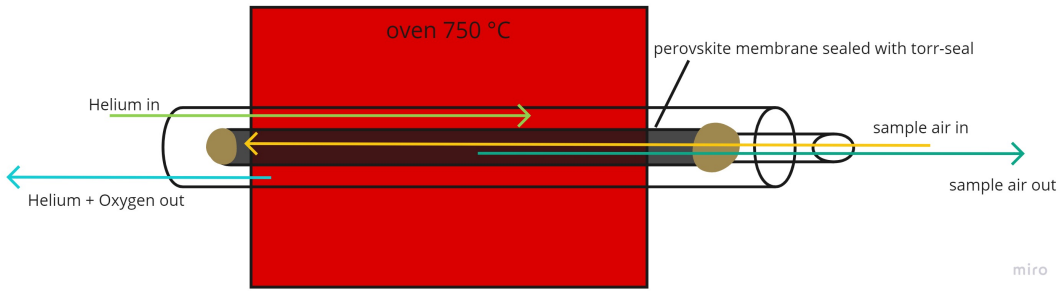

Figure 2.4: The oven in which oxygen is removed from the sample.

The capillary through which the sample leaves the membrane ends in the center where the helium is flushed in. As the partial pressure difference is presumably highest where the oxygen get flushed away directly, the permeation rate might be highest at that point, so the sample should contain the least amount of oxygen.

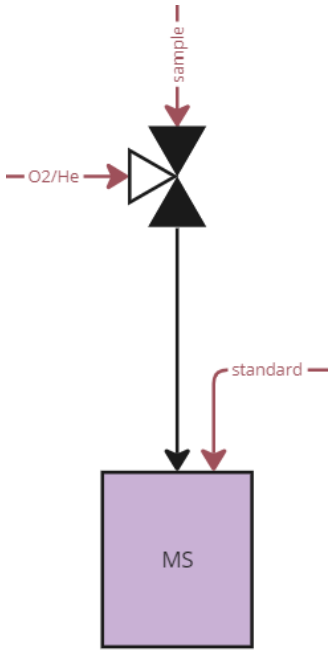

Figure 2.5: A setup to switch between the line inside and outside of the membrane. Each line enters one pneumatic valve respectively and then both connect with a T. The left line is outside, so it contains oxygen and helium. The upper capillary is the one on the inside of the membrane, which contains the oxygen-depleted sample. In which direction the valve is set is indicated by the black triangles. The capillary coming to the MS from the right is the standard line.

Directly in front of the MS, a valve was added (figure 2.5) to be able to switch between the line outside and inside the oven. Ideally, it could then be chosen whether $\delta^{18}O$ or the oxygen-depleted sample is to be measured.

2.3 Experiments

2.3.1 Leak in the membrane

During the initial measurements, the results were indicating that the membrane might have a small leak. Therefore, several ratios and deltas were calculated for those measurements on the outside of the membrane on AIR configuration at 400 °C. Finally, it was decided to open up the oven to be able to look at the membrane, but due to its fragility it broke during the process. Searching for another membrane, a shorter one with one closed end was found and attached instead. The advantage of this setup was, that the left end didn't have to be sealed and consequently only one side stuck out of the oven and was exposed to lower temperatures. However, this second setup only lasted shortly and before proper measurements could be taken, the membrane broke again. The results of this short period indicated though that a shorter membrane had a faster permeation rate and thus could offer a faster reaction time on the O_2/He line.

2.3.2 Testing the ceramics paste

A vacuum tight sealing material was then searched, which could withstand the high temperatures, in order to seal one end and recreate this setup with a short membrane. Previously, a gold paste was used (Larsen, 2018), which was not usable anymore and too expensive to purchase again. Therefore, a paste of *High Temperature Chemical Set Cement* by the producer *Omega Engineering Inc.* was tested if it was vacuum-tight. The product was in form of powder and had to be mixed with water to create the paste. Afterwards, it was applied on a glass tube of the same kind as the membrane followed by the instruction of the manufacturer. Three steps of drying were necessary to ensure it can withstand the oven temperatures:

1. 18 hours at room temperature
2. 4 hours at 80 °C
2. 4 hours at 104 °C

Then, the glass tube was attached at the right side of the oven and measured whether air would get in. An argon-filled bottle was used in addition to blow the gas onto the sealed end and see if the values increased on the MS. However, as will be discussed later in the discussion (chapter 4), the paste was not vaccum tight and no other suitable sealing material was found. Finally, another piece of membrane was installed in the same way as the initial one, with both ends sticking out of the oven and closed with Torr-seal.

2.3.3 Oxygen Permeation

To investigate the temperature dependency of oxygen permeation through the perovskite membrane, measurements were taken while rising the temperature for four different combinations of configuration and line:

1. O2 configuration on the MS (measuring the oxygen isotopes) and on the O_2 line (outside the membrane; the blue capillary in figure 2.4 or the left capillary in figure 2.5)
2. O2 configuration and on the N_2/Ar line (inside the membrane; the dark green capillary in figure 2.4 or the upper capillary in figure 2.5)
3. AIR configuration on the O_2 line
4. AIR configuration on the N_2/Ar line

Measurements were taken for approximately 10 min for each temperature and combination.

2.3.4 Oven Temperature

The temperature inside the oven is regulated via a PID thermocouple stick with the tip in the center. This setup ensures the temperature set at the regulator (usually 750 °C) is reached in the middle. However, as the membrane extends further than both ends of the oven and the oxygen permeation is linked to the temperature, the latter was measured at different positions in the oven. The thermocouple measures at the tip, but probably heats up the further it is inside the oven so measurements were taken from both ends.

2.3.5 Reaction Time

To measure the reaction time of the CFA on the O_2 line, the valve was switched between lab air and N_2/Ar as seen in fig 2.6. It is important to know how long the gas takes to pass through the line to be able to link the measurements of the MS to the corresponding position of the ice core on the melt-head and hence, the depth and timescale of the results. By switching from lab air to the N_2/Ar line, it was possible to measure the amount of time from the moment of turning the valve to the moment when the values changed on the MS.

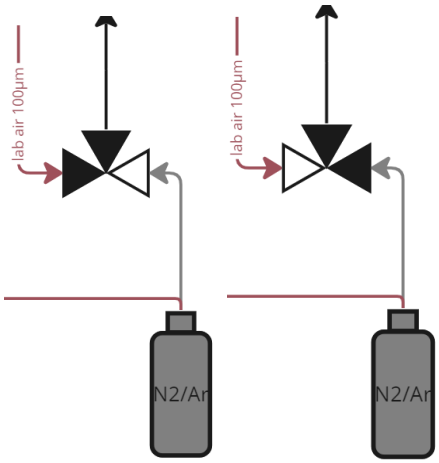

Figure 2.6: Switching the valve between lab air and a bottle filled with with a nitrogen/argon mixture in order to measure the reaction time of the CFA setup on the outside of the membrane.

2.3.6 Measuring firn air

To investigate whether the membrane causes fractionation as the O_2 diffuses through it, gases with different properties were measured. Air can have different isotopic compositions due to fractionating processes as explained in chapter 1.0.4. Therefore, various bottles from the North Greenland Eemian deep ice core (NEEM) and the North Greenland Ice Core Project (NGRIP), with previously measured $\delta^{18}O$ values were used. The bottles contained surface firn air and air from below close-off depth (were the gas gets trapped in bubbles, see section 1.0.2). The results could then be compared to the known values of the earlier measurements.

The bottles were attached instead of the N_2/Ar which is connected to the lab air capillary (shortly after the membrane at the end of the water line, see figure 2.3). An additional adjustment to the system was made: the line initially

transporting the standard to the MS was instead connected to the sample line before the oven. Henceforth, the valves at the MS could be switched to either measure gas from the bottle that has passed through the membrane or gas that has not. The setup can be seen below in figure 2.7.

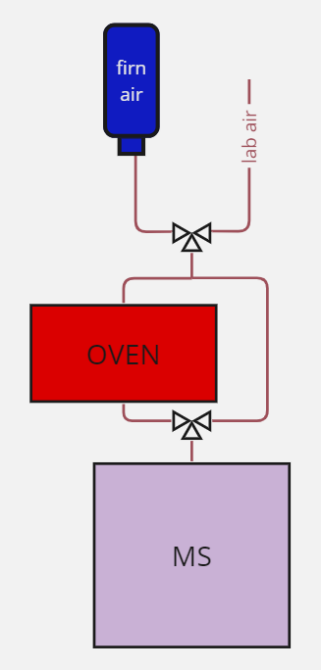

Figure 2.7: Schematic setup for measuring lab air and firn air before and after the membrane. The first valve can be switched between lab and firn air, the second between sample that has passed through the oven and sample that has not.

Firstly, NEEM bottles were measured. As they were older than 10 years and had possibly leaked over time, the methane concentrations were compared at the beginning. There were two bottles with previously measured concentrations seen in table 2.4.

Table 2.4: Values of two NEEM bottles for depth and methane.

	6122-66	912-91
Depth	69.80 m	71.40 m
CH_4 concentration	1588.6 ppb	1458.3 ppb

The measurements of the NEEM bottles indicated that they were in fact not tight and had been contaminated. From that point onward, only two bottles from EGRIP were used (labeled CIC_04 and CIC_9). The bottles had been measured before; the data is shown in table 2.5.

Table 2.5: Values of two EGRIP bottles for depth, methane and carbon dioxide concentrations and $\delta^{18}O$.

	CIC_04	CIC_9
Depth	60.86 m	7.83 m
CO_2 concentration	380 ppm	409.9 ppm
CH_4 concentration	1854.5 ppb	1934.5 ppb
$\delta^{18}O$	0.58 ‰	0.8 ‰

Firstly, the bottle CIC_04 was measured against lab air to compare their isotopic composition to the known data. This bottle was chosen as the air is from a lower depth and the delta is therefore greater and more easily to compare.
On the O_2 line outside of the membrane, oxygen isotopes were measured afterwards. Thereby, the two EGRIP bottles were attached and compared to lab air.

3 Results

3.1 Leak in the membrane

During the first measurements, the results were indicating that the membrane might have had a leak.

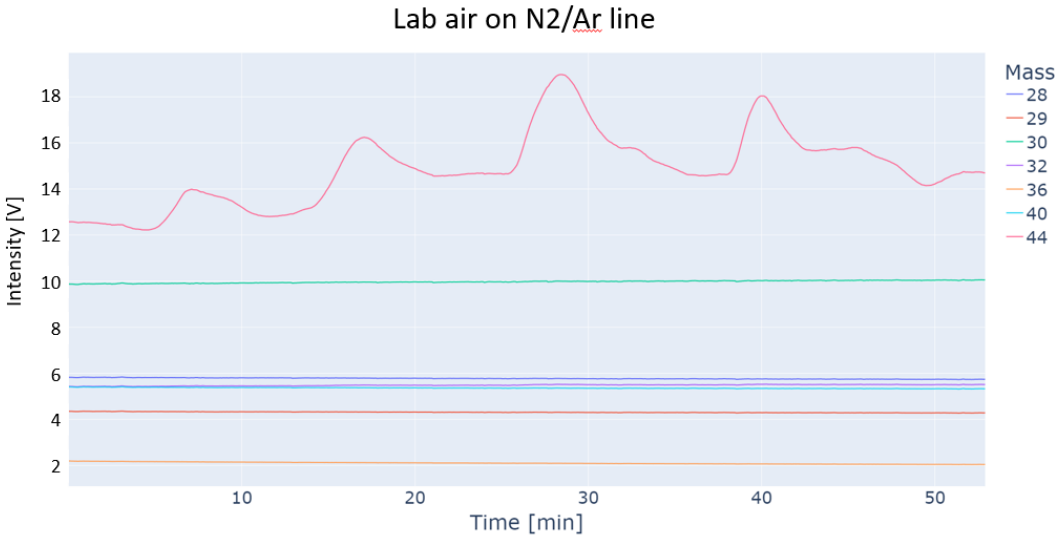

Figure 3.1: Measurements of lab air on the sample line inside the membrane on AIR configuration. Mass 44 varies greatly throughout the entire plot, all other masses seem stable.

The values on the N_2/Ar line seem to be stable except for mass 44, which varies greatly due to changing lab air concentrations. Mass 30 values are comparably high. Firstly, a variety of molecules that are not analyzed in this thesis have this mass, while only two are listed as an example in table 2.1. Secondly, this mass has a higher amplification than most of the molecules relevant for the research of this project.

As the absolute values might change only slightly with a small leak, ratios and deltas were calculated for the measurements as shown in figure 3.2.

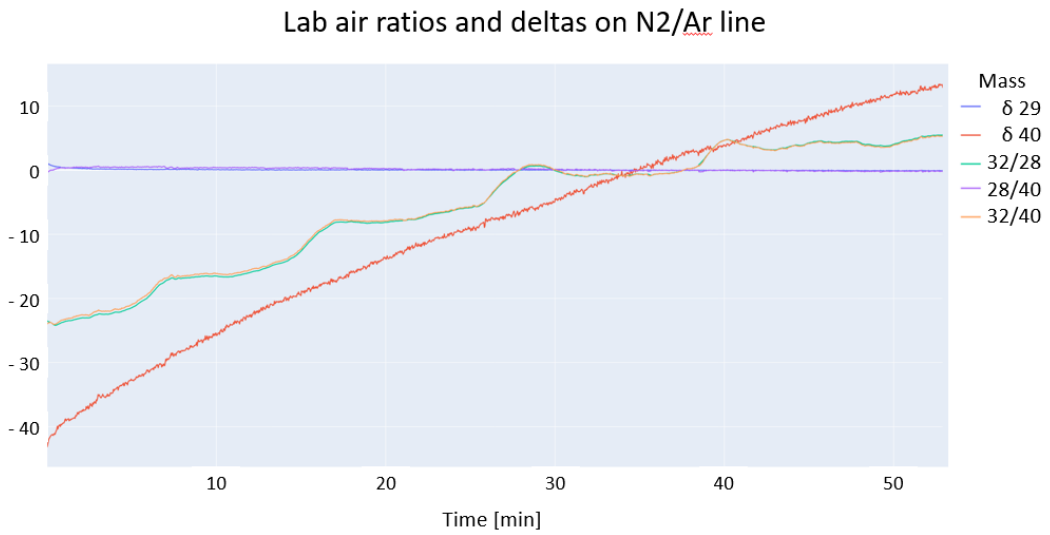

Figure 3.2: Different ratio and delta values from the measurements of the previous plot. Deltas are given in per-mille, while the ratios are unitless. The ratios with oxygen (32/28 and 32/40) increase constantly, but oscillate irregularly. $\delta^{40}Ar$ values increase steadily.

The ratios including mass 32 increase throughout the plot, but vary greatly. $\delta^{40}Ar$ values incline steadily. The ratio of mass 28 to 40 and $\delta^{29}N_2$ are close to zero throughout the plot.

3.2 Testing the ceramic paste

Figure 3.3: Measuring the air only connected to the glass tube sealed with the ceramics paste.

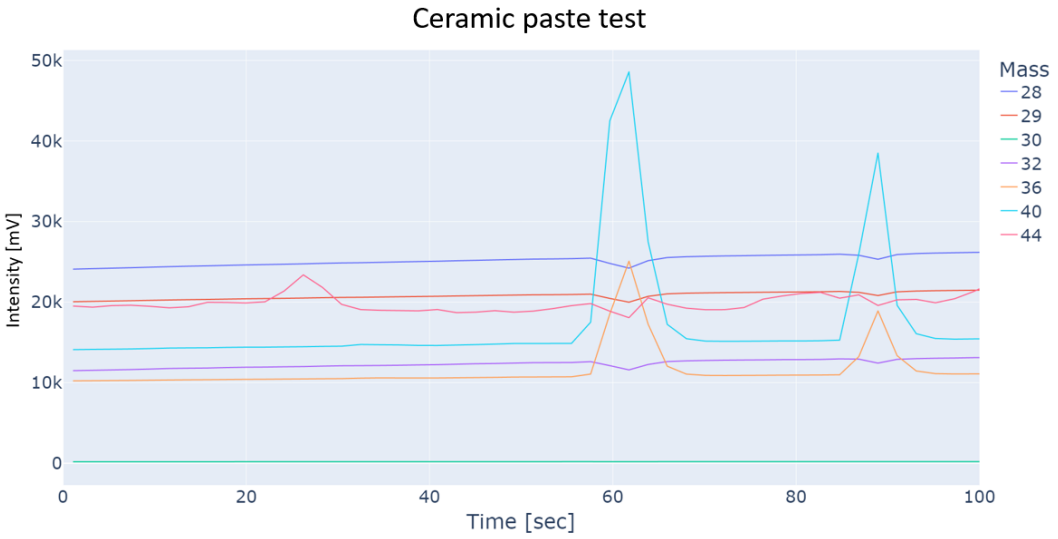

Figure 3.3 shows the measurements of testing whether the ceramic paste would seal the glass tube vacuum-tight. To observe whether argon entered the tube, one has to look at the values of the masses 36 and 40, which are the two stable argon isotopes measured. At 60 and around 90 seconds, the values increase distinctly. Additionally, a small decline in the other gases can be seen simultaneously, while mass 44 (CO_2) varies clearly throughout the entire measurement.

3.3 Oxygen Permeation

The following plots show averaged values for each mass (and some deltas) at every temperature step respectively.

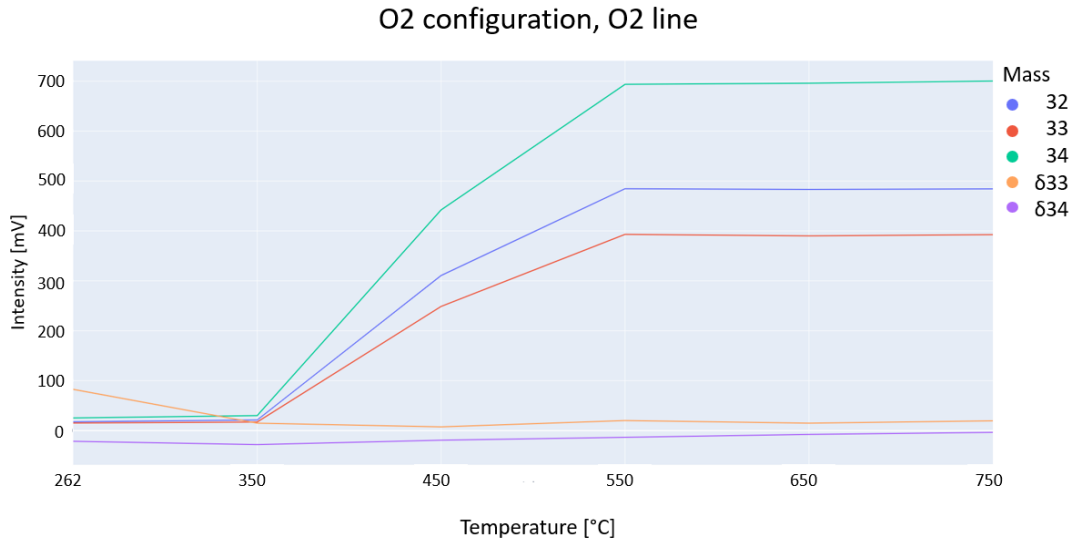

Figure 3.4: Measurements on O2 configuration on the O_2 line outside the membrane at various temperatures. Deltas are in per-mille. Masses 32, 33 and 34 all increase after 350 °C and reach their maximum values after 550 °C.

All three oxygen isotopes are almost non-present outside of the membrane at temperatures below 350 °C and reach a maximum signal of 700 mV (^{34}O) above 550 °C. Mass 34 shows the highest values, which is cause by the amplification settings explained in 2.1.1. It is important to keep in mind, that the values do nor represent relative or absolute abundances, but values can only be ultimately compared when taking the respective resistors into account. $\delta^{33}O$ decreases clearly from 262 to 350 °C, while $\delta^{34}O$ increases slowly and steadily with rising temperatures above 350 °C.

Inside the membrane, oxygen declines rapidly above 350 °C until it is nearly zero at temperatures below 650 °C. The maximum value for O^{34} is around 6000 mV, which is more than 8 times the value measured outside of the membrane. The value for δO^{33} increases above 550 °C and peaks at 650 °C. δO^{34} behaves similarly, but with much lower values.

The only oxygen isotope measured on the Air configuration is ^{32}O, which shows a line similar to the previous plots. The line starts increasing at around

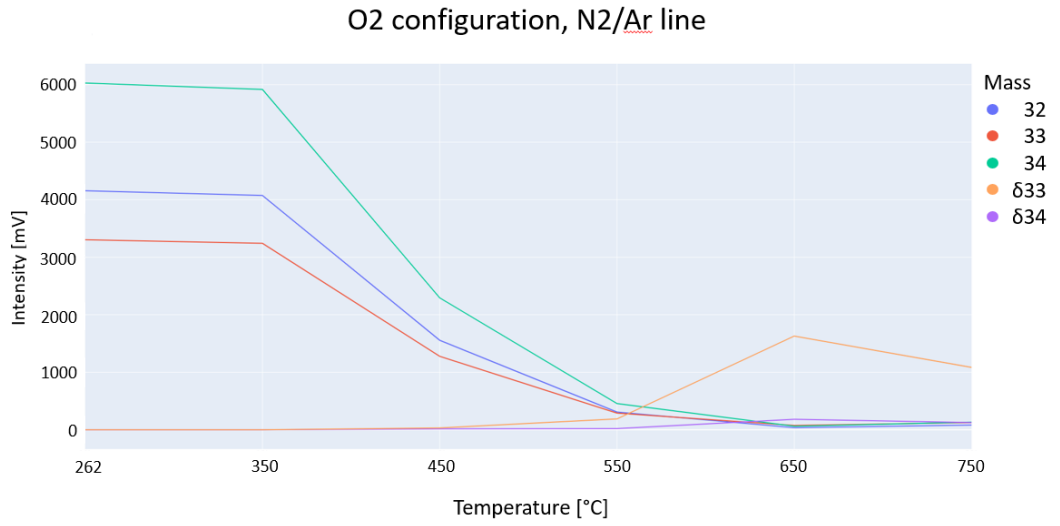

Figure 3.5: Measurements on O2 configuration on the N_2/Ar line inside the membrane at various temperatures. Deltas are in per-mille. All oxygen isotopes decline with time, while the deltas increase above 550 °C.

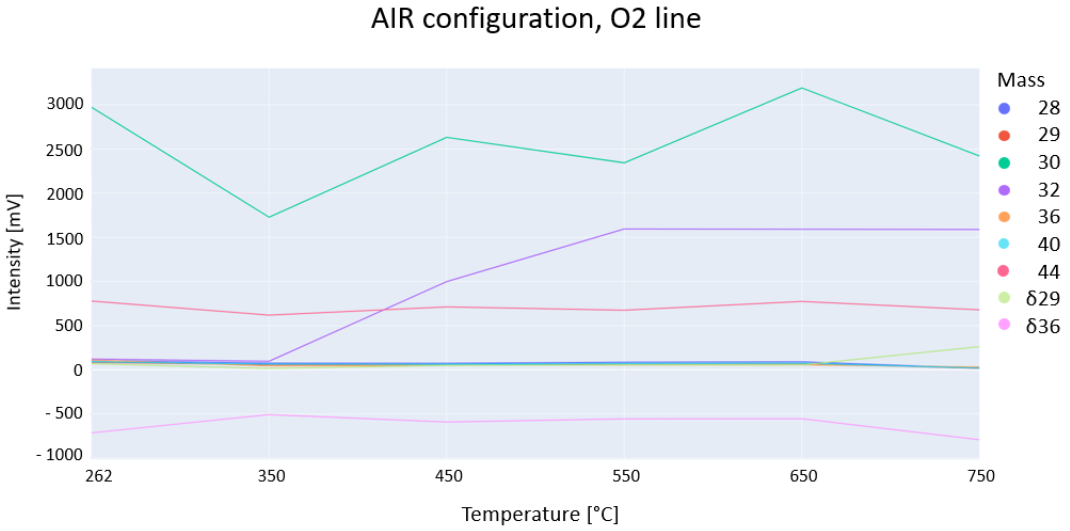

Figure 3.6: Measurements on Air configuration on the O_2 line outside the membrane at various temperatures. Deltas are in per-mille. Mass 32 increases with time, mass 30 varies greatly and mass 44 is stable but higher than the rest of the masses, which are all close to zero.

350 °C and reaches its maximum of about 1500 V at 550 °C. Ideally, only oxygen would be measured on this line, however, also the masses 30 and 44 are detected. δN^{29} is close to zero and increases slightly at 750 °C, while δAr^{36} is far below zero.

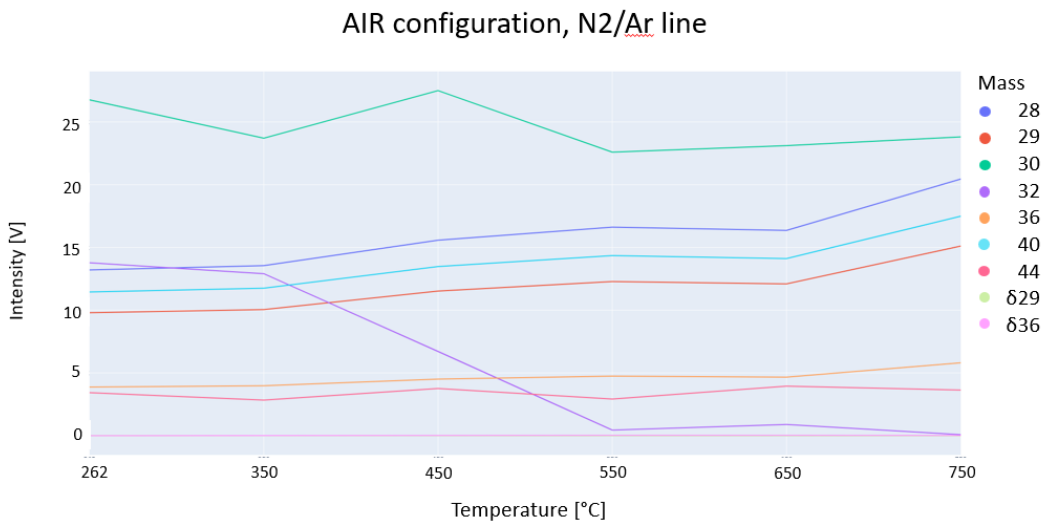

Figure 3.7: Measurements on Air configuration on the N_2/Ar line outside the membrane at various temperatures. Deltas are in per-mille. Most masses increase, while mass 32 declines above 350 °C.

As in the previous graphs, oxygen values decrease clearly between 350 and 550 °C, while the curves of the masses 28, 29 and rise continuously. Both deltas are constantly near zero and mass 44 is varying slightly throughout the plot. The values on the y-axes are given in volt instead of millivolt like the previous graphs. This indicates how the abundance of all gases is highest on the N_2/Ar line.

3.4 Oven Temperature

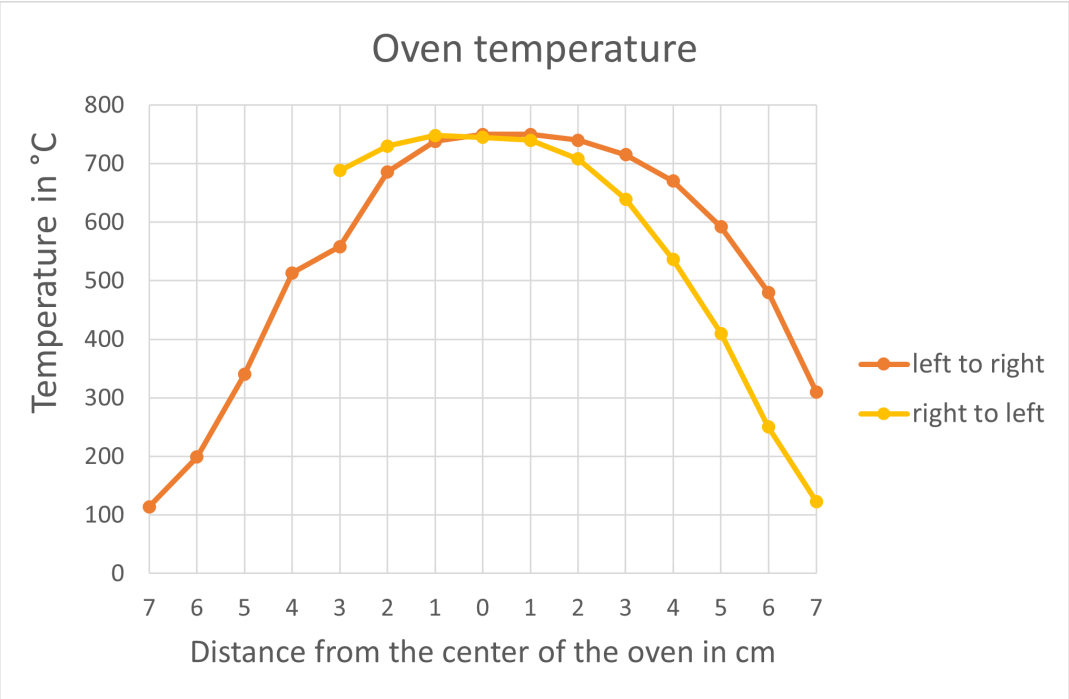

Figure 3.8: Temperature inside the oven measured from both ends. The temperature is set to 750 °C.

Figure 3.8 shows, that the set temperature of 750 °C is reached at the center of the oven. Two to three centimeters from the middle, the temperature drops under 700 °C and with four to six centimeter distance, it decreases to less than 500 °C.

3.5 Reaction time

The reaction time of the line is defined in the following as the period between the switching of the valve and the stabilization of the values measured by the MS. It was suspected, that the membrane prolongs this period as the oxygen has to pass through and therefore, measurements were taken from outside the membrane on the O_2/He line. Firstly, the valve was set to lab air and the MS was set to measure oxygen isotopes. The first switch of the valve to the N_2/Ar line was at around 1215 min, after which it took approximately until 1250 min, so a total of 35 min to stabilize. However, the lines don't become completely horizontal but rather keep on decreasing very slightly. Afterwards, the valve was set to measure lab air again and the values stabilize after around

20 min. This process was repeated once more with similar results, switching from lab air to N_2/Ar taking a longer time than vice versa.

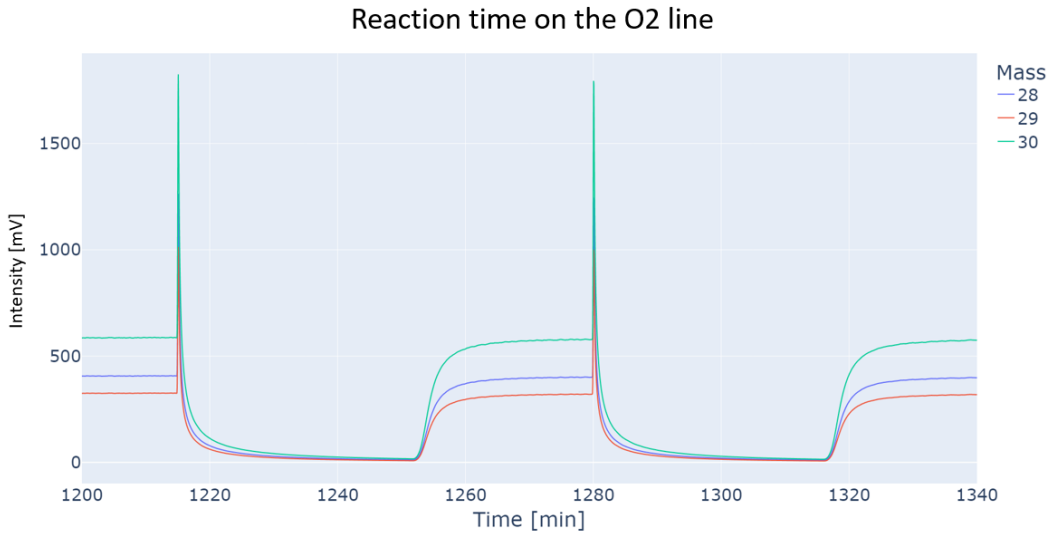

Figure 3.9: Switching the valve between lab air and the N_2/Ar line in order to measure the reaction time of the CFA setup. Oxygen abundance slowly approaches zero when the valve is switched to N_2/Ar, and increase faster when set back to lab air.

3.6 Measuring firn air

Firstly, the methane concentrations of the two NEEM bottles were measured.

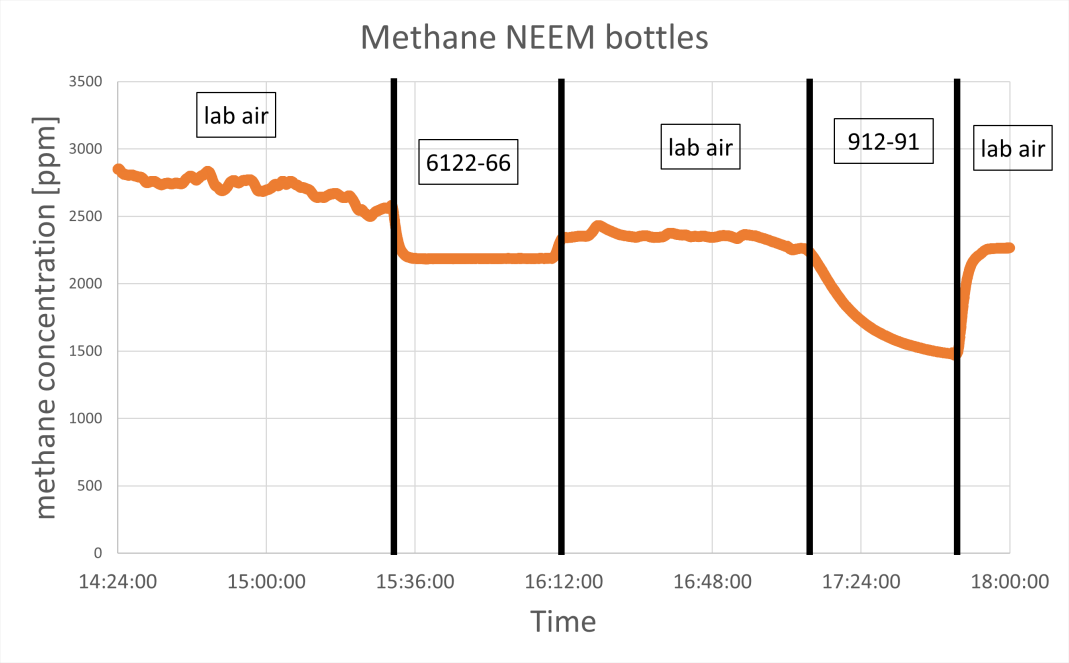

Figure 3.10: Measuring lab air against two firn air bottles from NEEM. Black vertical lines indicate a switch. The lab air concentrations are between 2000 and 3000 ppm, and slightly decreasing throughout the plot. Both bottles show concentrations below 2500 ppm and more stable values.

It can be seen in figure 3.10, that the bottles have lower methane concentrations and their values vary less compared to lab air. After the switch (indicated by the black line), the values drop from above 2500 ppm to around 2200 ppm. By switching back to lab air, the concentrations increase, but are lower compared to the previous lab air values. When the second bottle is attached, the values drop much slower than with the first bottle and reach 1500 ppm. The last switch to lab air causes a quick incline above 2200 ppm.
None of the bottles shows the concentration of the previous measurements from table 2.4.

Afterwards, EGRIP bottles were measured and $\delta^{34}O$ calculated.

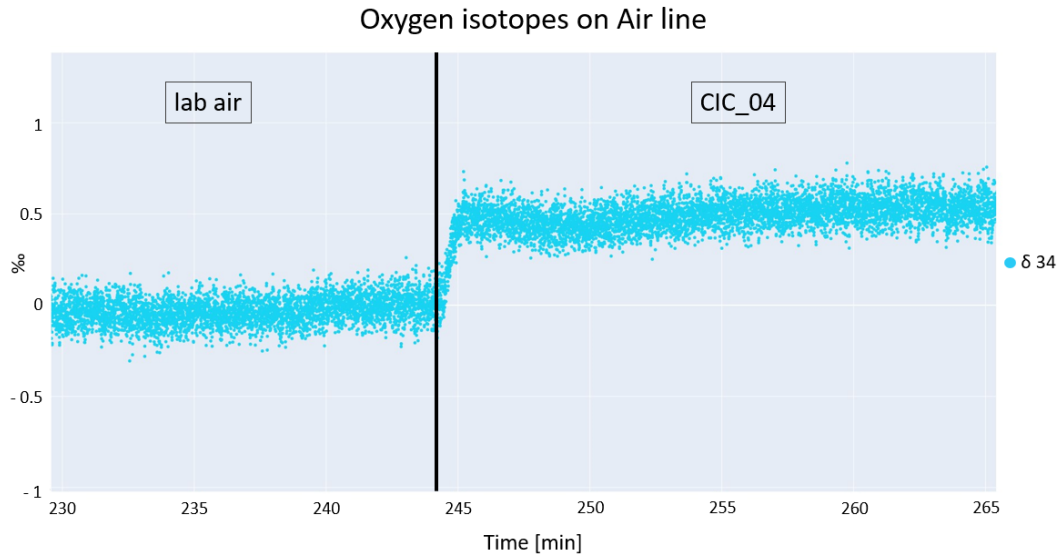

Figure 3.11: Measuring $\delta^{34}O$ of lab air against the firn air bottle CIC_04. Switch of the valve is indicated by the black of vertical line. Values change shortly after the switch and rise form around 0 to approximately 0.5. Directly after the rapid increase, there is a slight dip for several minutes, after which the values stabilize again at slightly above 0.5.

Figure 3.11 shows lab air measured against the CIC_04 EGRIP bottle to compare the $\delta^{34}O$ values. Lab air values were used as a standard to calculate an average delta for the firn air bottle

$$\delta^{34}O(CIC\_04) = 0.49 \pm 0.15.$$

The black vertical line indicates the switch from lab to firn air, which is followed by values clearly increasing. Shortly after, the values drop slightly before they balance approximately 10 min after the valve was switched.

To compare those values to oxygen passing through the membrane, figure 3.12 shows both bottles compared to lab air. The switching from bottle to lab air via valve is indicated by the black vertical lines. The values do not change correlating to a switch, but rather stay continuous throughout the entire measurement.

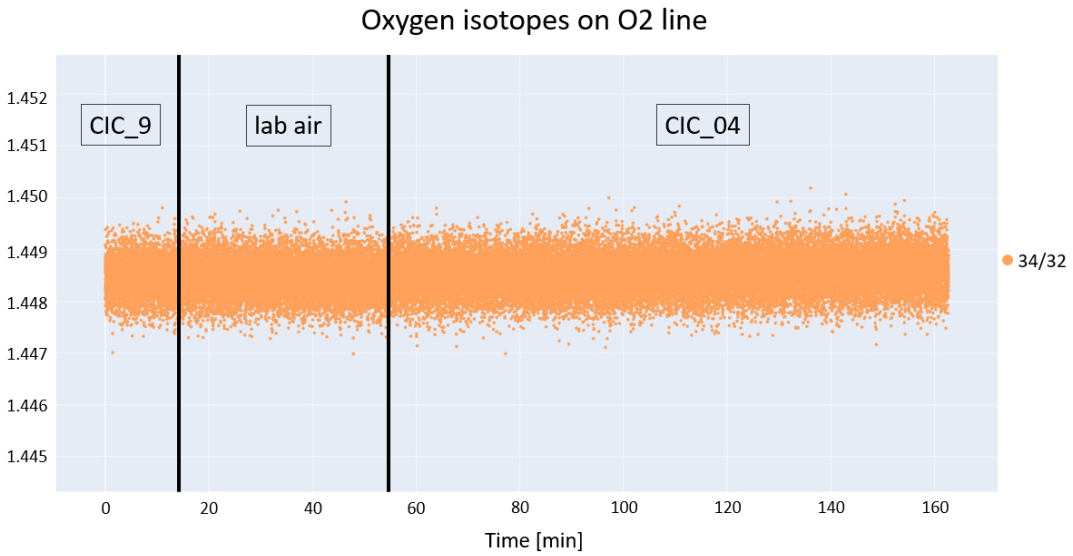

Figure 3.12: The ratio between mass 32 and mass 34 measured on the O_2 line for two different EGRIP bottles and lab air. A black vertical line indicates a switch via valve. The values do not change in correlation to the switching between different samples.

The values for $\delta^{34}O$ do not change between the EGRIP bottles and lab air.

4 Discussion

4.1 Leak in the membrane

The increase in the O_2/N_2 and O_2/Ar ratios and $\delta^{40}Ar$ in the figures 3.1 and 3.2 are most likely caused by a leak in the membrane. The partial pressures of nitrogen and argon are higher inside the membrane than outside, so if there is a leak both gases would diffuse towards the outside, while the partial pressure of oxygen can be expected to be rather stable or decreasing. Either the permeation through the membrane is balanced out by the diffusion back into the membrane via the leak, or total oxygen concentration is just declining. While argon and nitrogen concentrations decrease over time, the ratios compared to oxygen would increase in both cases, as seen in the figures. Furthermore, lighter isotopes are more likely to diffuse first through the leak, which can be the reason for the $\delta^{40}Ar$ value to be low in the beginning. However, as heavier isotopes are then more abundant on the inside, they start diffusing more with time and delta values increase.
It was finally decided to open up the oven to have a look at the membrane and potentially replace it. During this process, the membrane broke and had to be replaced anyways.

4.2 Testing the ceramics paste

The distinct increase in mass 36 and 40 in graph 3.3 demonstrates how argon entered the glass tube, indicating that the ceramic paste is in fact not vacuum-tight. The slight decrease in the values of the other masses can be explained

by the fact that the additional argon replaces the other gases in the mixture. Another indicator for the ceramic paste being permeable for air is the variation in CO_2 values. The carbon dioxide concentration in the lab air varies constantly with the presence and absence of people and their distance to the gas inlet.

The following experiments were then executed with the third membrane and the same setup as the initial one.

4.3 Oxygen Permeation

The results from the figures 3.4 and 3.6 indicate oxygen starts diffusing through the membrane at a temperature around 350 °C and is at its maximum at around 650 °C. However, it is crucial to note that there is clearly more oxygen measured inside compared to the outside of the membrane and oxygen values stay steady already after 550 °C on the O_2 line. The reason could be the wall of the membrane itself filling up with oxygen, though the difference in values might not be explained with this phenomenon alone.
The isotopes all have different resistors, as explained in 2.1.1. However, those just influence their absolute values and don't influence the relative shape of the curve.
The high $\delta^{33}O$ and $\delta^{34}O$ values in figure 3.4 and 3.5 occur simultaneously with low oxygen values for all isotopes. This means that the values are too slow to lead to accurate results, but are mostly influenced by noise. For $\delta^{34}O$ on the O_2 line however, it is distinguishable how the values slowly increase with temperatures above 350 °C. This could be explained if lighter isotopes diffuse faster through the membrane than the heavier ones. Firstly, most of the oxygen passing through is ^{32}O, but as temperatures rise, this effect gets smaller and heavier isotopes diffuse increasingly, driving up the delta.
On the Air Configuration, oxygen can be seen to start passing through the membrane after 350 °C and reaching maximum permeation at around 550 °C. CO_2 is set to high amplification, which is hence most likely the only reason for its high values. Nitrogen does not seem to vary correlating to the temperature, suggesting that it is only traces from the line directly in front of the MS. The masses used to calculate both deltas are close to zero, hence the calculated values are not expressive.
Figure 3.6 shows oxygen to decline between 350 and 550 °C, which correlates

with the previous graphs. While oxygen become less abundant on the inside of the membrane, the curves of almost all other gases rise as their relative abundance increases. Carbon dioxide abundance is linked to strongly varying values inside the lab air, but soothed out due to the trap with liquid nitrogen, which freezes out most of it.
Overall, in can be concluded, that oxygen diffusion through the perovskite membrane seems to reach a maximum after 550 to 650 °C.

4.4 Oven Temperature

The oven temperature set with the PID is only reached in the center of the oven and then quickly declines towards both ends. As it was first measured from left to right, it became obvious that the measuring stick shows higher temperatures when being further in the oven. Therefore, the measurement from the right to the left side were stopped shortly after the center and the lower of the two measured temperatures is likely more accurate. The results indicate that the oxygen may not diffuse at the same pace everywhere on the membrane, but rather have a fast permeation rate in the center and not permeate at all on the outer ends. From the figures 3.7, 3.6, 3.5 and 3.4 it can be concluded, that oxygen permeation does not occur at temperatures below 350 °C, indicating that the oxygen accumulates in the membrane at the ends of the oven. The continuous flow should prevent a long residence time, but it is likely, that the measurements are impacted by this dynamic. In addition, the position of the capillary trough which helium and oxygen flow towards the mass spectrometer (figure 2.4) could explain the low values on the O_2 line. As the oxygen does not enter the line directly at the position were it most likely leaves the membrane, it can diffuse further inside the glass tube. A possible solution would be to replace the latter with a smaller tube, but none with the right measurements could be found.

4.5 Reaction time

Figure 3.9 clearly shows that the values take at least 20 minutes to stabilize after switching between the two lines, which might be caused by the membrane retaining the oxygen. It has previously been observed, that oxygen is being left in the membrane, which led to the abandonment of a project involving ^{17}O measurements by Reutenauer (2016). It has been proven that permeability is increased for thinner membranes (Schiestel et al., 2005). Therefore, the retention of oxygen might cause long reaction times, as the bulk diffusion through comparably thick membrane walls slows down the permeation process. It could be, that the membrane has to get entirely saturated with oxygen first, before the molecules get released on the outer wall again. As the oxygen permeation is dependant on a partial pressure difference between inside and outside of the membrane, it might be possible, that no bulk diffusion occurs if there is no or too little oxygen abundant on the inner side. This is the case when switching from lab air containing oxygen to the N_2/Ar line. It could be, that as the nitrogen and argon mixture enter the membrane, the partial pressure of oxygen decreases and permeation slows down drastically, causing a long stabilization time. The opposite effect occurs when turning the valve to lab air and oxygen enters the membrane, increasing its partial pressure. While the short membrane was in use, the reaction time seemed to be significantly shorter, though no measurements were taken before it broke. It is possible though, that the smaller volume and moreover the fact that a smaller part of the membrane was at a lower temperature might have caused faster oxygen permeation.
Figure 3.11 shows how quickly the values change and stabilize when oxygen is continuously measured, but with different delta values. As the partial pressure does not decrease inside the membrane, permeation does not slow down and the reaction time is shorter.
Moreover, it would be interesting to measure the reaction time of the setup inside the membrane, to investigate it for the part of the sample, that does not permeate.

4.6 Measuring firn air

The measurements of the NEEM bottles were not comparable to the available data from table 2.4. The methane concentrations of both were higher than what has been previously measured. Hence, the initial hypothesis, that the bottles might have leaked throughout the years seems to be plausible. From that point onward, only EGRIP bottles were used for delta measurements.

As known from the data about both EGRIP bottles and previous measurements, it was expected to see a difference in $\delta^{34}O$ values of around 0.58 ‰. The calculated value from fig 3.11 is 0.49 $\pm$ 0.15 ‰ and therefore comparable, though the error is relatively high (one third of the value). The small decrease in $\delta^{34}O$ after switching the valve is most likely caused by a too small flow after opening the bottle. With too little sample flowing into the MS, no accurate delta values can be calculated. After a few minutes, the flow was adjusted and values stabilized.
However, when the oxygen passing through the membrane was measured on the O_2 line, the fractionation did not differ between air from the bottle and air from the lab. Delta values were not calculated, as the ratio already shows no variance in samples. These results indicate, that the oven set-up fractionates the oxygen to an extend where no difference in the delta values between lab and firn air can be observed. This could be caused by the heavier isotopes diffusing slower than the lighter ones. Additionally, the aforementioned temperature dependency of the permeation process and the fact that the membrane only reaches above 350 °C at the center of the oven could have an impact. If the oxygen either accumulates at the ends of the membrane or moreover, in the outer glass tube, different isotopes might have varying residence times. Hence, the final delta values might be defined by the permeation process itself and furthermore, the samples might get mixed inside the membrane and the outer glass tube. Hence, it is not possible to measure the oxygen isotope composition of samples on the O_2 line.

4.7 Future research suggestions

Firstly, the current membrane in use is the last one available at the institute currently and it is suggested to purchase new ones. Extracting oxygen through perovskite membranes is a continuous research topic for various reasons and it might be, that current technologies are improved and new membranes have a higher oxygen permeability (Buck et al., 2022; Buck et al., 2021). Furthermore, it can be worth it to purchase membranes that are closed on one end like the one from the second setup. Perovskite membranes however exist with different chemical compositions and are usually produced for other purposes such as oxygen production (Jiang et al., 2010). It is worth mentioning, that not all might be usable for the purpose of extraction oxygen isotopes form ice core samples, even with increased permeation fluxes.
The reaction time was specifically measured on the O_2 line while switching between lab air and the N_2/Ar mixture, which does not sufficiently reflect the reaction time for a sample with different isotopic compositions (e.g. an ice core). Figure 3.11 shows a much quicker reaction, which further hints to the fact that a slow reaction time would not be a problem when measuring oxygen deltas form ice cores. However, as all these experiments might be interesting to further study the permeation through the membrane, the results of this project mostly suggest that the oxygen gets fractionated by the membrane. It is therefore not advised to try measuring the oxygen that has diffused through the membrane, but rather investigate on other research questions.

5 Conclusion

The results indicate that oxygen permeation starts at around 350 °C and reaches a maximum after 550 °C. Furthermore, diffusion most likely does not occur over the entire surface of the membrane, but predominately in the center of the oven, where the temperature is high enough. Further from the center, the temperature drops quickly below 350 °C and oxygen might accumulate inside of the membrane instead of diffusing. The reaction time when switching between lab air and an N_2/Ar mixture was measured to be up to 35 min until values stabilized. However, other results indicate, that the reaction time is much quicker when switching between samples that all contain air, as permeation is dependant on a higher partial pressure of oxygen on the inside. It is advised to purchase new membranes, as the current one is the last one available at PICE. Then it might be advantageous, to find a shorter and thinner one, which could lead to a faster diffusion rate. Another possibility is a smaller surrounding glass tube, which would further cause a smaller dead volume. Additionally, the membrane should be closed on one end, as it is difficult to find suitable materials to seal an open end.
Concluding the findings about oxygen isotope measurements on the outside of the membrane: it is not possible. The membrane seems to affect the isotopes differently and causes fractionation. Samples with different isotopic compositions cannot be distinguished once the oxygen has diffused through the membrane.

Bibliography

Bender, M., Sowers, T., & Labeyrie, L. (1994). The dole effect and its variations during the last 130,000 years as measured in the vostok ice core. *Global Biogeochemical Cycles*, *8*(3), 363–376. https://doi.org/10.1029/94GB00724

Blunier, T., & Leuenberger, M. (2008). Stable isotopes - isoskript.

Blunier, T., & Schwander, J. (2000). Gas enclosure in ice : Age difference and fractionation, 307–326. http://hdl.handle.net/2115/32473

Bradley, R. S. (2000). Past global changes and their significance for the future. *Quaternary Science Reviews*, *19*(1), 391–402. https://doi.org/10.1016/S0277-3791(99)00071-2

Buck, F., Bunjaku, O., Caro, J., & Schiestel, T. (2022). High-flux CO2-stable oxygen transport hollow fiber membranes through surface engineering. *Journal of the European Ceramic Society*, *42*(4), 1537–1547. https://doi.org/10.1016/j.jeurceramsoc.2021.11.040

Buck, F., Feldhoff, A., Caro, J., & Schiestel, T. (2021). Permeation improvement of LCCF hollow fiber membranes by spinning and sintering optimization. *Separation and Purification Technology*, *259*, 118023. https://doi.org/10.1016/j.seppur.2020.118023

Buizert, C., Martinerie, P., Petrenko, V. V., Severinghaus, J. P., Trudinger, C. M., Witrant, E., Rosen, J. L., Orsi, A. J., Rubino, M., Etheridge, D. M., Steele, L. P., Hogan, C., Laube, J. C., Sturges, W. T., Levchenko, V. A., Smith, A. M., Levin, I., Conway, T. J., Dlugokencky, E. J., … Blunier, T. (2012). Gas transport in firn: Multiple-tracer characterisation and model intercomparison for NEEM, northern greenland [Publisher: Copernicus Publications]. *Atmos. Chem. Phys.*, *12*(9), 4259–4277. https://doi.org/10.5194/acp-12-4259-2012

Craig, H., Horibe, Y., & Sowers, T. (1988). Gravitational separation of gases and isotopes in polar ice caps. *Science*, *242*(4886), 1675–1678. https://doi.org/10.1126/science.242.4886.1675

Cuffey, K., & Paterson, W. S. B. (2010). *The physics of glaciers* (4th ed) [OCLC: ocn488732494]. Butterworth-Heinemann/Elsevier.

Dahl-Jensen, D., Gundestrup, N. S., Miller, H., Watanabe, O., Johnsen, S. J., Steffensen, J. P., Clausen, H. B., Svensson, A., & Larsen, L. B. (2002). The NorthGRIP deep drilling programme. *Annals of Glaciology*, *35*, 1–4. https://doi.org/10.3189/172756402781817275

Dansgaard, W. (2012). Stable isotopes in precipitation. *Tellus A: Dynamic Meteorology and Oceanography*, *16*(4), 436. https://doi.org/10.3402/tellusa.v16i4.8993

Dole, M. (1935). The relative atomic weight of oxygen in water and in air. *Journal of the American Chemical Society*, *57*(12), 2731.

Grew, K. E., & Ibbs, T. (1952). Thermal diffusion in gases. *Cambridge University Press*.

Guillevic, M. (2013, November). *Characterisation of rapid climate changes through isotope analyses of ice and entrapped air in the NEEM ice core* (Doctoral dissertation). University of Copenhagen, Faculty of Science; Université de Versailles Saint Quentin en Yvelines (UVSQ). https://theses.hal.science/tel-01277038/file/Guillevic_PhDthesis_2nd_edition_3feb2014.pdf

Herron, M. M., & Langway, C. C. (1980). Firn densification: An empirical model. *Journal of Glaciology*, *25*(93), 373–385. https://doi.org/10.3189/S0022143000015239

Jiang, H., Liang, F., Czuprat, O., Efimov, K., Feldhoff, A., Schirrmeister, S., Schiestel, T., Wang, H., & Caro, J. (2010). Hydrogen production by water dissociation in surface-modified BaCoxFeyZr1xyO3 hollow-fiber membrane reactor with improved oxygen permeation. *Chemistry - A European Journal*, *16*(26), 7898–7903. https://doi.org/10.1002/chem.200902494

Larsen, B. X. N. (2018, January 4). *Oxygen removal from air of atmospheric composition - by a membrane technology* (Doctoral dissertation). Copenhagen University, Niels Bohr institute, Physics of ice climate and earth. Copenhagen.

Liang, F., Jiang, H., Schiestel, T., & Caro, J. (2010). High-purity oxygen production from air using perovskite hollow fiber membranes. *Industrial*

& Engineering Chemistry Research, *49*(19), 9377–9384. https://doi.org/10.1021/ie101311g

Liisberg, J. B. (2020, May 25). *Abrupt climate change and the nitrogen cycle* (Doctoral dissertation). Copenhagen University, Niels Bohr institute, Physics of ice climate and earth. Copenhagen.

Malaizé, B., Paillard, D., Jouzel, J., & Raynaud, D. (1999). The dole effect over the last two glacial-interglacial cycles. *Journal of Geophysical Research: Atmospheres*, *104*, 14199–14208. https://doi.org/10.1029/1999JD900116

Pederzani, S., & Britton, K. (2019). Oxygen isotopes in bioarchaeology: Principles and applications, challenges and opportunities. *Earth-Science Reviews*, *188*, 77–107. https://doi.org/10.1016/j.earscirev.2018.11.005

Rasmussen, S. O., Abbott, P. M., Blunier, T., Bourne, A. J., Brook, E., Buchardt, S. L., Buizert, C., Chappellaz, J., Clausen, H. B., Cook, E., Dahl-Jensen, D., Davies, S. M., Guillevic, M., Kipfstuhl, S., Laepple, T., Seierstad, I. K., Severinghaus, J. P., Steffensen, J. P., Stowasser, C., ... Winstrup, M. (2013). A first chronology for the north greenland eemian ice drilling (NEEM) ice core. *Climate of the Past*, *9*(6), 2713–2730. https://doi.org/10.5194/cp-9-2713-2013

Reutenauer, C. (2016). *Measuring the triple o2 isotopic composition of air trapped in ice cores and quantifying the causes of d18oatm millennial scale variations.* Copenhagen University, Centre for ice; climate.

Schiestel, T., Kilgus, M., Peter, S., Caspary, K., Wang, H., & Caro, J. (2005). Hollow fibre perovskite membranes for oxygen separation. *Journal of Membrane Science*, *258*(1), 1–4. https://doi.org/10.1016/j.memsci.2005.03.035

Schwander, J., Barnola, J.-M., Andrié, C., Leuenberger, M., Ludin, A., Raynaud, D., & Stauffer, B. (1993). The age of the air in the firn and the ice at summit, greenland. *Journal of Geophysical Research: Atmospheres*, *98*, 2831–2838. https://doi.org/10.1029/92JD02383

Severinghaus, J. P., Beaudette, R., Headly, M. A., Taylor, K., & Brook, E. J. (2009). Oxygen-18 of o $_2$ records the impact of abrupt climate change on the terrestrial biosphere. *Science*, *324*(5933), 1431–1434. https://doi.org/10.1126/science.1169473

Severinghaus, J. P., Grachev, A., & Battle, M. (2001). Thermal fractionation of air in polar firn by seasonal temperature gradients. *Geochemistry, Geophysics, Geosystems*, *2*(7), n/a–n/a. https://doi.org/10.1029/2000GC000146

Severinghaus, J. P., Sowers, T., Brook, E. J., Alley, R. B., & Bender, M. L. (1998). Timing of abrupt climate change at the end of the younger dryas interval from thermally fractionated gases in polar ice. *Nature*, *391*(6663), 141–146. https://doi.org/10.1038/34346

Sowers, T., Bender, M., Raynaud, D., & Korotkevich, Y. S. (1992). 15n of n2 in air trapped in polar ice: A tracer of gas transport in the firn and a possible constraint on ice age-gas age differences. *Journal of Geophysical Research: Atmospheres*, *97*, 15683–15697.

Sunarso, J., Baumann, S., Serra, J., Meulenberg, W., Liu, S., Lin, Y., & Diniz Da Costa, J. (2008). Mixed ionic–electronic conducting (MIEC) ceramic-based membranes for oxygen separation. *Journal of Membrane Science*, *320*(1), 13–41. https://doi.org/10.1016/j.memsci.2008.03.074

Yang, W., Wang, H., Zhu, X., & Lin, L. (2005). Development and application of oxygen permeable membrane in selective oxidation of light alkanes. *Topics in Catalysis*, *35*(1), 155–167. https://doi.org/10.1007/s11244-005-3820-6